

Equal-energy-sharing ($e,2e$) ionizing collisions in argon

D. K. Waterhouse,¹ I. E. McCarthy,² and J. F. Williams¹

¹Centre for Atomic, Molecular and Surface Physics, Physics Department, The University of Western Australia, Perth, WA 6907, Australia

²Physics Department, Flinders University, Adelaide, SA 5042, Australia

(Received 15 July 1997)

Triple differential cross sections (TDCS) of the argon $3s$ and $3p$ outer shells were obtained from electron-impact ionization ($e,2e$) experiments with coplanar equal-energy sharing scattering geometries. The advantages of a new asymmetric equal-energy-scattering geometry are described. Data are reported for incident electron energies of 2020, 1220, 620, and 420 eV. Measurements extend to the high-binding momentum region of the TDCS. The data are compared with recent distorted-wave calculations, with a view to determining the range of validity of the models for coplanar equal-energy-sharing kinematics. [S1050-2947(98)03805-0]

PACS number(s): 34.80.Dp

I. INTRODUCTION

Selected kinematics in ($e,2e$) measurements of triple differential scattering cross sections (TDCS) of selected atomic states can probe details of atomic structure [1,2], or of the collision dynamics [3]. In an ($e,2e$) collision an incident electron $e_0(E_0, \mathbf{k}_0)$ ionizes an electron from a target atom or molecule and the outgoing electrons are conventionally labeled scattered $e_s(E_s, \mathbf{k}_s)$, and (with lower energy) ejected $e_e(E_e, \mathbf{k}_e)$, where each has an energy E and momentum \mathbf{k} with the relevant subscripts. The kinematics of an ($e,2e$) event are fully determined, except (usually) for the electron spin. By energy conservation, the separation energy E_{sep} of the bound target electron is $E_{\text{sep}} = E_0 - E_s - E_e$, and by momentum conservation the target electron binding momentum is $q = |\mathbf{k}_0 - \mathbf{k}_s - \mathbf{k}_e|$. The momentum transfer in an ($e,2e$) collision is $\mathbf{K} = \mathbf{k}_0 - \mathbf{k}_s$ and is largest when the outgoing electrons have equal energies.

Many quantum-mechanical scattering models are used for the ($e,2e$) interaction with varying degrees of success. Two of the more successful models are the impulse approximation and the Born approximation. Within these approximations the incident and outgoing electrons are described by plane waves, leading to the PWIA and PWBA models, or by distorted waves, giving the DWIA and DWBA scattering models.

The plane-wave models essentially ignore electron interactions with the target atom and the residual ion, and are expected to be valid only when the electron energies are high and the target and residual ion can be treated as spectators that take no part in the event. In this way the ($e,2e$) collision can be treated as a direct knock-out of the target electron by the incident electron. The PWIA is qualitatively good up to about $q=1$ a.u., even far from bound-electron Bethe ridge [4] kinematics.

In the distorted-wave models the electron wave functions are calculated in the appropriate distorting potential that includes the electron interactions with the target and residual ion. The distorted-wave models have been shown to be more generally applicable, and are often valid even for quite low electron energies. The DWIA model [1] is known to be a

good approximation up to about $q=2$ a.u. for both noncoplanar and Bethe ridge conditions, with incident energies greater than about 1000 eV. The DWBA is good near the Bethe ridge, and is quite good, at least qualitatively [5], far from the Bethe ridge. The distorted-wave models tend to be less good when the incident electron energy is low and the outgoing electrons are detected in coplanar symmetric equal-energy conditions.

For coplanar symmetric kinematics, scattered and ejected electrons are detected with equal energies $E = E_s = E_e$, at equal angles on opposite sides of the incident electron beam, and the incident electron energy is $E_0 = 2E + E_{\text{sep}}$. The probability of close electron-electron collisions is maximized and the electron-electron interactions become relatively important. This geometry provides a good test of scattering approximations because the bound electron momentum q and the momentum transfer \mathbf{K} vary by large amounts.

Distortion effects become relatively important in the high- q region of the wave function that represents essentially the inner region of the atom. The validity of distorted-wave models in the high- q region of the wave functions is not well established, mostly because the TDCS are relatively small and are difficult to measure with suitable statistical accuracy. In some instances, for example, for 1200-eV incident energy and about 600-eV outgoing electron energy, the available experimental data [6,7] differ, and a definitive statement about the applicability of the models in the high- q region cannot be made. The high- q region was studied [8] with coplanar symmetric scattering at 200-eV incident energy, with a view to determining the roles of postcollision interactions between the outgoing electrons and elastic scattering of the incident electron from the nucleus prior to ionization (which is represented in distorted-wave models). Recently, Rioual *et al.*, [9] cited a number of investigations of He, Ne, Xe, and Ar, and of selected molecules, that used symmetric energy sharing kinematics. The helium data were matched well by the DWBA calculations [10].

Argon is a heavier atom and the structure is more complex than helium, so distortion effects might be expected to become more important sooner. Measurements on Xe [11] and Ne [12] showed the DWBA model calculations were not

as good for heavier targets at low energies. DWBA calculations for the high- q region were in reasonable agreement with recent low-energy symmetric ($e,2e$) measurements on argon [13], but the agreement at smaller angles was quite poor.

New data are reported here from coplanar equal-energy-sharing ($e,2e$) measurements of the argon $3s^{-1}$ ($E_{\text{sep}}=29.24$ eV) and $3p^{-1}$ ($E_{\text{sep}}=15.76$ eV) atomic states with a range of incident electron energies from 420 to 2020 eV, with data extending well into the high- q region of the TDCS. The data are compared with the DWIA and DWBA models, with a view to determining the validity of the models for coplanar equal-energy-sharing kinematics. Some limitations of the models are exposed, particularly when the electron-electron interactions are relatively strong at low incident energies and small relative scattering angles. The coplanar asymmetric equal-energy-sharing geometry has not been used often, and some of the advantages of this geometry will be described. Section II briefly describes the distorted-wave models, and Sec. III describes the multichannel ($e,2e$) spectrometer used for this work. Calibrating ($e,2e$) measurements of the helium $1s^{-1}$ state are discussed. Section IV discusses data from the coplanar equal-energy-sharing measurements on argon $3s^{-1}$ and $3p^{-1}$ states.

II. DISTORTED-WAVE MODELS

The ($e,2e$) TDCS for electron-impact ionization of a single electron from an inert target atom is

$$\frac{d^5\sigma}{d\Omega_s d\Omega_e dE_e} = (2\pi)^4 \frac{k_s k_e}{k_0} \sum_{av} |T_f(\mathbf{k}_s, \mathbf{k}_e, \mathbf{k}_0)|^2 \quad (1)$$

with

$$T_f(\mathbf{k}_s, \mathbf{k}_e, \mathbf{k}_0) = \langle \mathbf{k}_s, \mathbf{k}_e | T | \alpha \mathbf{k}_0 \rangle. \quad (2)$$

The expression in Eq. (1) includes a sum over final and average over initial magnetic and spin state degeneracies, and $d\Omega = \sin\theta d\theta d\phi$. The T_f matrix in Eq. (2) is the reaction amplitude, it couples the initial states α and the final states. T_f includes interactions between the incident and target electrons and the nucleus. It is the part of the TDCS that is the subject of approximation.

In the distorted-wave Born approximation calculation

$$T_f \equiv \langle \chi^-(\mathbf{k}_s) \chi^-(\mathbf{k}_e) | \nu_3 | \alpha \chi^+(\mathbf{k}_0) \rangle. \quad (3)$$

The electron-electron potential ν_3 is responsible for ionization. The initial state α contains an electron bound to the atom core with separation energy E_{sep} . The distorted waves for the incident and scattered electrons, $\chi^+(\mathbf{k}_0)$ and $\chi^-(\mathbf{k}_s)$, respectively, are calculated in a potential $U_1 = \langle \alpha | \nu_1 + \nu_3 | \alpha \rangle$. The scattered electron interacts with the inert core via the potential ν_1 , with the addition of a spin-averaged exchange term. A suitable potential ν_2 that describes the interaction of the outgoing ‘‘ejected’’ electron with the target’s ion core is used to calculate $\chi^-(\mathbf{k}_e)$. For a many-electron atom the Hartree-Fock potential is suitable.

In the plane-wave impulse approximation it is assumed that electron interactions with the core can be ignored, but the electron-electron Coulomb interaction is treated exactly

using the T matrix t_3 for the Coulomb potential ν_3 . Because the interaction is translationally invariant the impulse approximation permits factorization of the reaction amplitude T_f into a collision factor and a structure term. The impulse approximation is usually only valid for high electron kinetic energies, but this condition is relaxed by replacing the plane waves with distorted waves in the structure factor, keeping the factorization. The distorted waves are constructed in the same way as in the DWBA, and the DWIA T -matrix element is

$$T_f \equiv \langle \mathbf{k}' | t_3 | \mathbf{k} \rangle \langle \chi^-(\mathbf{k}_s) \chi^-(\mathbf{k}_e) | \alpha \chi^+(\mathbf{k}_0) \rangle, \quad (4)$$

where $\mathbf{k} = \frac{1}{2}(\mathbf{k}_s - \mathbf{k}_e)$ and $\mathbf{k}' = \frac{1}{2}(\mathbf{k}_0 - \mathbf{q})$. The parameter \mathbf{q} is the target electron momentum, calculated by momentum conservation, its magnitude was given earlier. The factorization approximation in the DWIA is not exact, and the electron-electron collision cannot be treated as a free collision except on or very near the Bethe ridge. As the DWIA does not properly account for the electron-ion interactions it is expected to be a relatively poor approximation in the high- q region of the TDCS.

The DWIA takes account of postcollision electron-electron interaction (PCI) effects, since the electron-electron T matrix describes the whole interaction. In contrast, the DWBA does not take account of the PCI effects, but they can be included by using effective charges to calculate the distorted waves. Sometimes the Gamow factor, $\Gamma(\nu) = 2\pi\nu / [\exp(2\pi\nu) - 1]$, where $\nu = 1/|\mathbf{k}_s - \mathbf{k}_e|$ is used as a scaling factor in the DWBA to approximate PCI effects. The Gamow factor is a factor in the T matrix.

III. EXPERIMENT

Measurements of argon $3s^{-1}$ and $3p^{-1}$ state TDCS have often been restricted to $q < 2$ a.u. by the limiting detection efficiency of the apparatus. A multiparameter coincidence detection system [14] allowed simultaneous acquisition of data from the $3s^{-1}$ and $3p^{-1}$ energy-loss peaks, and significantly reduced the uncertainty associated with each data point for a given acquisition time. The two electron energy analyzers were identical 180° electrostatic analyzers with input optics designed to operate with a deceleration ratio of up to 50:1. The crucial feature of each analyzer that made it ideal for the TDCS measurements was the output of the position-sensitive detector formed by two microchannel plates and a resistive anode. Each resistive anode image was an energy-dispersed scattered electron signal with an energy range of about 30% of the pass energy of the analyzer. The optimization and operation of the apparatus are discussed elsewhere [15].

The acceptance angle of each detector was 2.7° , and the coincidence energy resolution was 2.5 ± 0.2 eV, sufficient to separate the argon $3p^{-1}$ state at 15.76 eV and the $3s^{-1}$ state at 29.24 eV. The coincidence time resolution was 0.8 ns, with a time walk [16] of less than 0.12 ns per histogram cell resulting from different electron paths through the analyzer. The background signal intensity from accidental coincidences was small in equal-energy-sharing geometries, and the signal-to-noise ratio was usually better than 10:1. The target gas was admitted through a 0.3-mm-diameter single

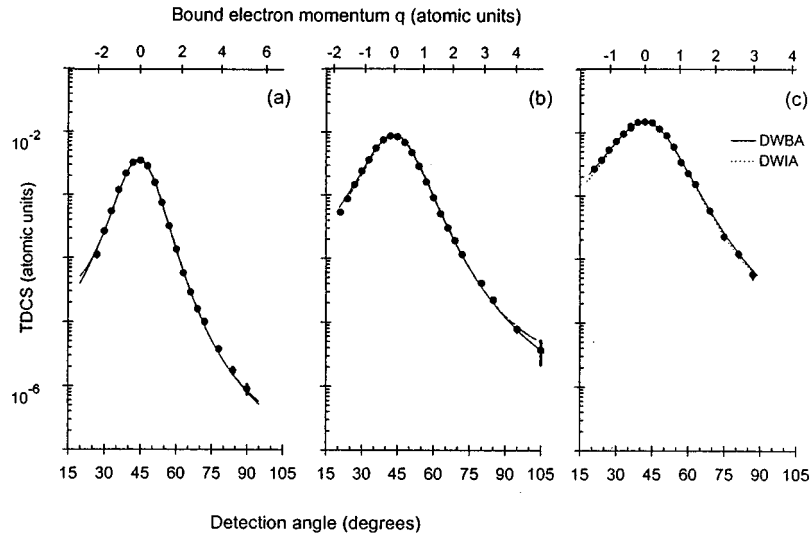


FIG. 1. Helium $1s^{-1}$ TDCS measured in coplanar asymmetric equal-energy-sharing geometry for incident electron energies of (a) 1220 eV, (b) 620 eV, and (c) 420 eV. The angle acceptances and energy resolution are folded into the calculated DWBA (—), and DWIA (----) TDCS.

orifice gas jet. The $4\text{-}\mu\text{A}$ incident electron beam had a diameter of less than 1 mm with small divergence at energies around 1000 eV, and an energy spread of about 0.75 eV. The beam broadened to more than 1.5 mm at 400 eV, but tests showed that the ejected electron analyzer viewed the same interaction volume from all detection angles.

Some of the measurements were done with coplanar equal energy sharing conditions, but with asymmetric scattering geometry in which the scattered electron detector was fixed on the bound-electron Bethe ridge at about 45° . The ejected electron detector was scanned through a range of angles on the opposite side of the incident beam, from 21° to 115° . Data were limited to the binary scattering peak because the detector dimensions prevented operation with both detectors on the same side of the incident electron beam. The equal-energy-sharing asymmetric scattering geometry offered the experimental advantages of a fixed reference signal from the scattered electron detector that was used to correct for variations in the target gas intensity or incident electron current. Another advantage was that this geometry had constant momentum resolution as the ejected electron detector was swept over the angular range of interest, in contrast to truly symmetric geometries where the momentum resolution varies significantly [17]. The momentum transfer \mathbf{K} is constant and electron exchange effects are small, so the Mott scattering factor remains constant. Also, the angular range for a given variation of q is broader by as much as a factor of two than for truly symmetric (energy and angle) measurements. This feature reduces the importance of small angular acceptances, and so improved the coincidence data acquisition rates for high q , where there was a need to test calculated TDCS data.

Double-differential cross section (DDCS) and TDCS data for particular experimental conditions were obtained simultaneously, and the DDCS data were used to normalize the TDCS data. The DDCS data were compared with a semi-empirical binary encounter model [18]. That model was only expected to be a good representation when the dipole interaction is small, such as for hydrogen and helium. The experi-

mental TDCS data are not absolute, but because the argon $3s^{-1}$ and $3p^{-1}$ TDCS were simultaneously obtained, the relative magnitudes could be compared easily. The argon data were scaled to obtain the best fit to the $3p^{-1}$ spectroscopic factor of 0.95 [1]. The TDCS of the observed $3s^{-1}$ state at 29.24 eV was then adjusted to match the scaled experimental intensity. The scaling factor required to achieve agreement between the calculated and observed $3s^{-1}$ TDCS is the spectroscopic factor for the $3s^{-1}$ state, known to be 0.55 when measured using non-coplanar symmetric kinematics [19]. The spectroscopic factors are independent of the incident energy.

IV. RESULTS

A. Characterization with helium

Helium is a suitable target to use when characterizing the performance of the ($e,2e$) apparatus, as the TDCS are relatively large and are well understood for intermediate and high incident electron energies. Some of the helium TDCS data acquired using coplanar asymmetric equal-energy-sharing kinematics are shown in Fig. 1, and compared with the distorted-wave model calculations. The incident electron energies were (a) 1220 eV, (b) 620 eV, and (c) 420 eV. The DWBA is shown in each plot as a solid line and the DWIA by a dotted line. The standard error is plotted for each data point, but often the uncertainty is smaller than the size of the data symbol. The experimental data were scaled to give the best visual fit to the calculated ($e,2e$) TDCS, and the vertical logarithmic scales in parts (a), (b), and (c) are identical.

A distinction between the distorted-wave Born and impulse approximations could not be made from the 1220-eV data; both appear equally applicable in the observed angular range. The distorted-wave models are expected to work quite well at 620 eV, and the data in Fig. 1(b) show the DWBA and DWIA are quite indistinguishable, even at high ejected

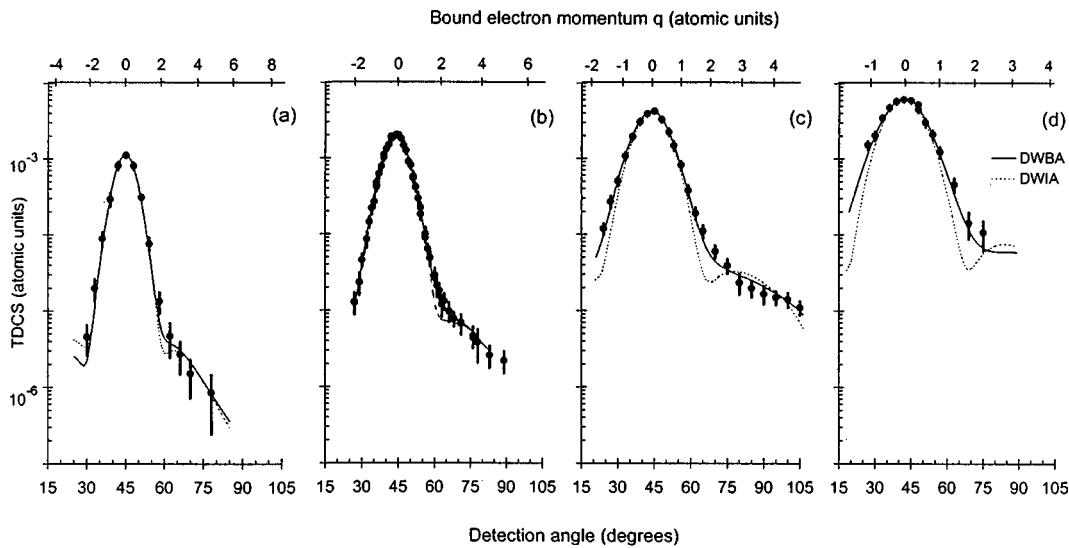


FIG. 2. Argon $3s^{-1}$ TDCS measured in coplanar asymmetric equal-energy-sharing geometry with incident electron energies of (a) 2020 eV, (b) 1220 eV, (c) 620 eV and (d) 420 eV. The angle acceptances and energy resolution are folded into the calculated DWBA (—), and DWIA (----) TDCS.

electron angles, corresponding to high q . The high statistical accuracy of the data obtained using this ($e,2e$) apparatus showed that in the 420-eV data the DWIA calculation underestimated slightly the TDCS for high q , and incorrectly predicted the direction of maximum momentum transfer \mathbf{K} (but by less than 1°), given by the position of the maximum in the TDCS.

B. Coplanar asymmetric equal-energy-sharing argon data

Measurements were conducted on the argon $3s^{-1}$ and $3p^{-1}$ states in coplanar asymmetric equal-energy-sharing geometry. The $3s^{-1}$ and $3p^{-1}$ data were acquired simultaneously, but are plotted separately for clarity. The data are compared with the DWBA and DWIA calculated TDCS.

Figures 2(a) and 3(a) show the $3s^{-1}$ and $3p^{-1}$ data, respectively, acquired with an incident energy of 2020 eV. The scattered and ejected electron energies were each 1000 eV. The $3s^{-1}$ data show a single peak at a detection angle corresponding to $q=0$ a.u. The $3p^{-1}$ data show two maxima resulting from binary collisions in which the target electron ejected from the atom has a particular momentum. The first peak at smaller angle, where $q < 0$ a.u., corresponds to the incident and target electrons having momenta in the same direction, and the second peak at larger angles, where $q > 0$ a.u., is where the incident and target electron momenta are in opposite directions. The minimum between the peaks corresponds to $q=0$ a.u., which has zero probability. The observation of the binding momentum q in the electron col-

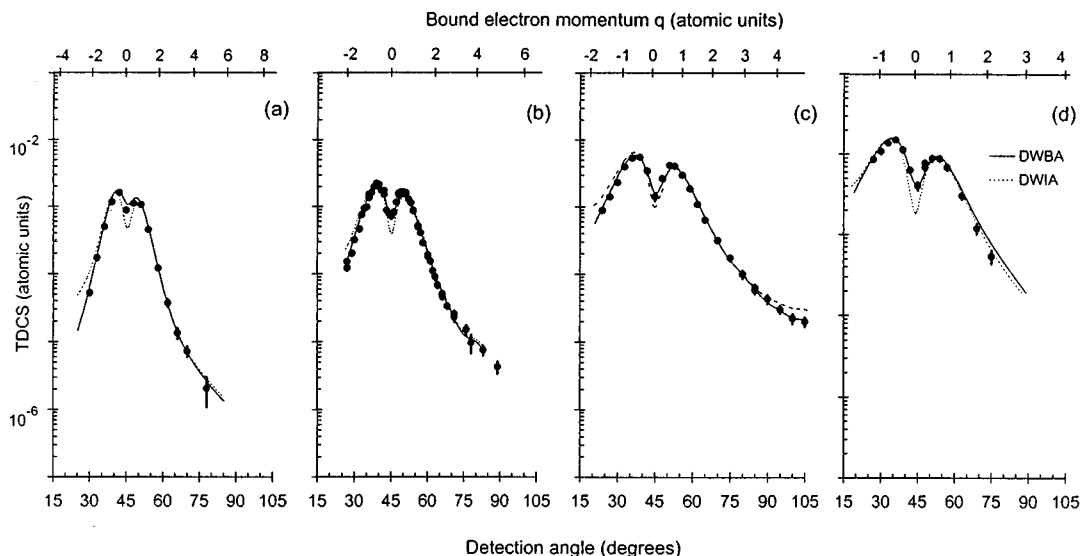


FIG. 3. Argon $3p^{-1}$ TDCS measured in coplanar asymmetric equal-energy-sharing geometry. The incident electron energies were (a) 2020 eV, (b) 1220 eV, (c) 620 eV, and (d) 420 eV. The angle acceptances and energy resolution are folded into the calculated DWBA (—), and DWIA (----) TDCS.

TABLE I. Coplanar asymmetric equal-energy-sharing kinematics fitting parameters used to obtain the best visual fit of the observed argon $3s^{-1}$ and $3p^{-1}$ TDCS to the calculated DWBA and DWIA TDCS for the listed incident electron energies. The numbers in () indicate the uncertainty in the last digit in the scaling and angle parameters.

Incident energy (eV)	DWBA			DWIA			Ratio of DWBA to DWIA
	Sum factor $3s$	$3p$	Angle shift (degrees)	Sum factor $3s$	$3p$	Angle shift (degrees)	
2000	0.50 (2)	0.95	0.1 (2)	0.51 (2)	0.95	0.0 (2)	1.49 (5)
1200	0.48 (2)	0.95	-0.6 (2)	0.50 (2)	0.95	-0.6 (2)	1.57 (4)
600	0.48 (2)	0.95	0.0 (2)	0.52 (2)	0.95	-0.4 (2)	1.74 (4)
400	0.52 (3)	0.95	-0.2 (2)	0.52 (3)	0.95	-0.8 (2)	2.03 (5)

lision is distorted by momentum transfers due to the remainder of the target, represented in the calculations by distorted waves. This reduces the depth of the minimum. The finite momentum resolution of the apparatus also reduces the depth. Our analysis suggests that even a slight azimuthal misalignment of the electron detectors (less than 0.1°) from the coplanar condition has a large effect on the momentum resolution in the region near $q=0$ a.u.

The $3s^{-1}$ and $3p^{-1}$ data were simultaneously acquired, providing an accurate method of comparing the relative TDCS magnitudes predicted by the model calculations. The $3p^{-1}$ data in Fig. 3 were scaled to provide the best visual fit to the $3p^{-1}$ DWBA TDCS for positive q , corresponding to detection angles θ_e greater than about 45° , and included the accepted spectroscopic factor of 0.95 [1]. In Fig. 2, the calculated $3s^{-1}$ TDCS were adjusted to obtain the best visual fit to the $3s^{-1}$ data. Similar data are shown in Figs. 2 and 3 for incident electron energies of (b) 1220 eV, (c) 620 eV, and (d) 420 eV. The experimentally determined $3s^{-1}$ spectroscopic factor for the observed state at 29.24 eV and the angular shifts required for the best visual fit between the observed TDCS and the TDCS using the DWIA and DWBA models are presented in Table I. In general for asymmetric equal energy-sharing kinematics, the observed $3s^{-1}$ spectroscopic factor was consistently about 10% smaller than expected, for all incident electron energies and for both scattering models. Also, the DWIA model predicted smaller TDCS than the DWBA, with the difference increasing as the incident energy decreased. Both models predicted the direction of maximum intensity quite well, given that there is uncertainty of $\pm 0.2^\circ$ in the detection angles. However, the DWIA TDCS needed to be shifted an additional -0.4° for the 620-eV and an extra -0.6° for the 420-eV data than the relevant DWBA calculated TDCS.

For 1220-eV incident energy, with scattered and ejected electron energies of 600 eV each, the data for the $3s^{-1}$ and $3p^{-1}$ peak are shown in Figs. 2(b) and 3(b). Similar measurements were reported previously [6,7] but different conclusions about the accuracy of the DWBA calculation were made in both cases, and were prompted mainly by differing experimental observations in the high- q region. These data, which extend to higher q than either of the previous measurements, show the DWBA calculation compares well, even at high q , for the $3s^{-1}$ and $3p^{-1}$ states.

When the incident electron energy was lowered to 620 eV and the scattered and ejected electron energies were 300 eV each, the TDCS data for the argon $3s^{-1}$ and $3p^{-1}$ states

shown in Figs. 2(c) and 3(c), respectively, were obtained. The shape of the DWBA calculation for the $3s^{-1}$ state agrees well with the data, but the DWIA calculation predicts a minimum in the $3s^{-1}$ cross section near 65° that is not present in the experimental data. The DWIA is expected to be less applicable as the energy of the electrons decreases because the factorization approximation becomes less good. Also, the impulse approximation is less valid for low electron energies as collisions are further from the free-electron condition. By simultaneously detecting the $3s^{-1}$ and $3p^{-1}$ TDCS, it was observed that the DWBA overestimates the $3p^{-1}$ TDCS by 5% at small scattering angles. The DWIA model does not predict the shape of the $3s^{-1}$ or $3p^{-1}$ distribution as well as the DWBA and, at ejected electron angles greater than about 85° , the DWIA overestimates the $3p^{-1}$ TDCS.

Data obtained with 420-eV incident energy are shown in Figs. 2(d) and 3(d). The agreement between the observed $3s^{-1}$ TDCS and the calculated DWBA TDCS is good, but the DWIA does not agree well. At small detection angles the agreement for the $3p^{-1}$ state between experiment and the calculated models is good, although the agreement at larger angles appears to deteriorate, and the DWIA is poor near $q=0$ a.u.

C. Coplanar symmetric argon data

Data for coplanar symmetric scattering TDCS were obtained with the same incident energies as the coplanar asymmetric equal energy sharing data discussed above. The symmetric energy-sharing geometry is expected to be the most revealing test of the DWBA as postcollision interactions in the final state become more important and, as noted earlier, the DWBA does not contain this interaction explicitly. The $3s^{-1}$ symmetric TDCS data were normalized to the $3s^{-1}$ asymmetric TDCS at the common detection angle of 45° . Data for the $3s^{-1}$ and $3p^{-1}$ states are plotted in Figs. 4 and 5, respectively, and are compared with the DWBA and DWIA calculations. Unfortunately the physical size of the electron detectors prevented measurements from extending to relative scattering angles less than about 64° (each detector at 32°), where the predicted TDCS show some interesting structure. The data were treated in the same way as the asymmetric data, and the spectroscopic factor of the observed $3s^{-1}$ state at 29.24 eV and the angular shifts required for the best visual data fits are presented in Table II. In general for symmetric equal-energy-sharing kinematics, the spectro-

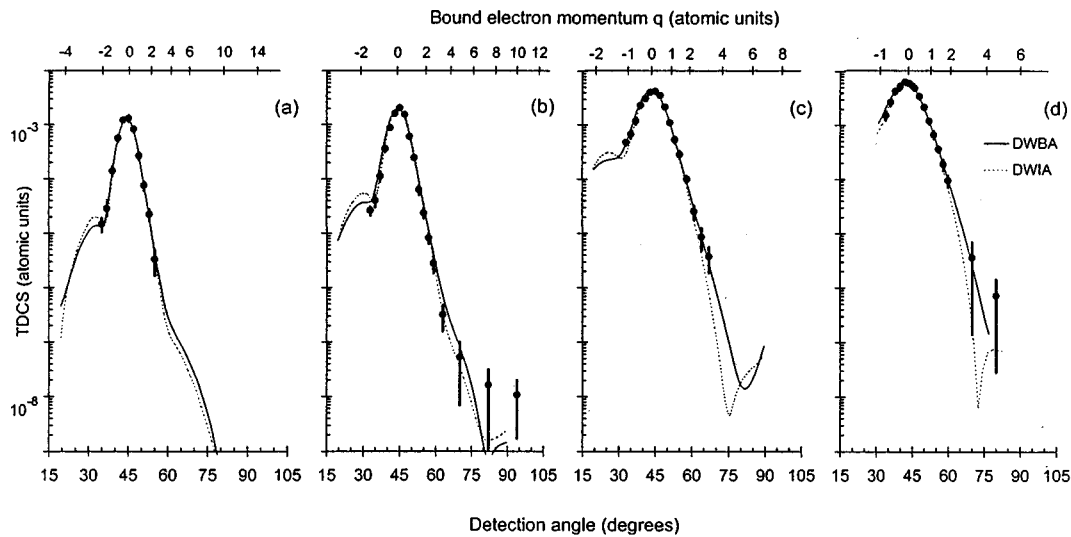


FIG. 4. Argon $3s^{-1}$ TDCS as for Fig. 2, but for coplanar symmetric scattering geometry.

scopic factor for the $3s^{-1}$ state was within one standard deviation of the expected value of 0.55. Once again the DWIA TDCS was smaller than the DWBA TDCS, and the difference increased as the incident energy decreased. Both models predicted the direction of maximum intensity well, except in the 420-eV data. As well, in the 420-eV data an additional shift of $-0.8 \pm 0.2^\circ$ in the calculated $3p^{-1}$ DWIA TDCS was required relative to the $3s^{-1}$ TDCS.

The observed TDCS for the $3s^{-1}$ and $3p^{-1}$ states of argon measured in coplanar symmetric geometry with an incident energy of 2020 eV is shown in Figs. 4(a) and 5(a), respectively. With such high incident electron energy even the DWIA is a good model. The angular range of the $3s^{-1}$ TDCS is only about two-thirds of the range measured in asymmetric geometry at the same incident energy. Data for an incident electron energy of 1220 eV, with scattered and ejected electron energies of 600 eV, are shown in Figs. 4(b) and 5(b). These data show the shapes of the DWBA and

DWIA calculation compare well for the $3s^{-1}$ and $3p^{-1}$ states, however, it appears that the apparatus limit was reached at high scattering angles where the observed $3s^{-1}$ TDCS flattens out. This may have prevented observation of the minimum predicted by both models. At angles greater than 70° the observed $3s^{-1}$ true coincidence signal rate was less than about 1×10^{-3} events/sec. Even at this relatively high incident electron energy the DWBA overestimates slightly the $3p^{-1}$ TDCS at small scattering angles, indicating that electron-electron interactions in the final state may already be important. Data for 620-eV incident electron energy are shown in Figs. 4(c) and 5(c), and for 420-eV incident energy in Figs. 4(d) and 5(d). The DWIA is a reasonable approximation in both instances, but it predicts deeper minima than observed at high q . In Figs. 5(c) and 5(d) the agreement of the DWBA with the observed $3p^{-1}$ TDCS where $q > 0$ a.u. is good, and the $3s^{-1}$ TDCS is predicted well at all angles for all incident electron energies.

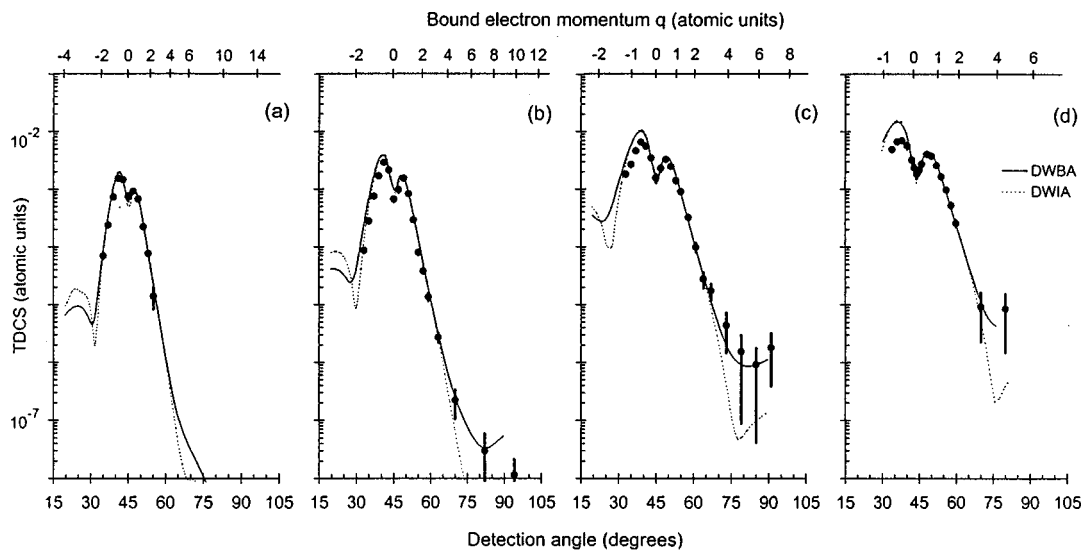


FIG. 5. Argon $3p^{-1}$ TDCS as for Fig. 3, but measured in coplanar symmetric scattering geometry.

TABLE II. As for Table I, but for coplanar symmetric geometry.

Incident energy (eV)	DWBA			DWIA			Ratio of DWBA to DWIA
	Sum factor 3s	3p	Angle shift (degrees)	Sum factor 3s	3p	Angle shift (degrees)	
2000	0.55 (2)	0.95	-0.4 (2)	0.53 (2)	0.95	-0.4 (2)	1.46 (4)
1200	0.56 (2)	0.95	-0.4 (2)	0.52 (2)	0.95	-0.2 (2)	1.52 (4)
600	0.56 (1)	0.95	-0.4 (2)	0.55 (1)	0.95	-0.6 (2)	1.74 (4)
400	0.52 (3)	0.95	-0.2 (2)	0.51 (3)	0.95	-1.3 (2)	2.15 (5)

It is notable that the DWIA and especially the DWBA fail for the $3p^{-1}$ state at scattering angles less than 45° where $q < 0$ a.u. Simultaneous acquisition of the $3s^{-1}$ and $3p^{-1}$ states using this apparatus provides the necessary evidence that the difference observed at small angles in the $3p^{-1}$ TDCS is more likely to originate from the calculations rather than from an experimental effect. The DWIA model could be expected to be poor due to breakdown of the impulse approximation at low energies. The inclusion of electron-ion interactions by using the DWBA does nothing to improve the comparison for $q < 0$ a.u., but the agreement for large $q > 0$ a.u. is significantly better. A similar situation was observed [20] in argon data on the Bethe ridge for an incident electron energy of 1000 eV and ejected electron energy of 120 eV, where the DWBA overestimated slightly the $3p^{-1}$ TDCS for small scattering angles where $q < 0$ a.u. The post-collision electron-electron interactions (PCI) are automatically included in the DWIA T matrix, but as noted earlier, the DWBA does not explicitly include the PCI effects following the collision. This omission is corrected to some extent by including the Gamow factor, described earlier, in the DWBA. The PCI effects would be largest for small relative scattering angles and would therefore tend to reduce the predicted TDCS at low angles if they could be properly accounted for. However, the experimental evidence suggests that the Gamow factor does not adequately account for PCI effects, and an alternative method of including PCI effects in the distorted-wave calculations may be required.

V. CONCLUSIONS

A systematic study of the argon $3s^{-1}$ and $3p^{-1}$ TDCS for coplanar equal-energy sharing kinematics has provided a good test of the validity of the DWBA and DWIA scattering models in this kinematics. In particular, coplanar symmetric data show the models systematically overestimated the TDCS of the argon $3p^{-1}$ state for $q < 0$ a.u. as the incident electron energy was decreased from 2020 to 420 eV. The agreement was worst at 420 eV, even when the Gamow factor was included in the DWBA model. The same data showed that the DWBA worked well in the same energy range for $q > 0$ a.u. for the $3p^{-1}$ state, and at all values of q for electrons ionized from the argon $3s$ and helium $1s$ orbitals. The DWBA and DWIA models were tested for the first time using a relatively new coplanar asymmetric equal-energy-sharing kinematics. The DWBA was in good agreement with the experimental data over the range 420–2020 eV incident electron energy, while agreement with the DWIA was limited to 2020 and 1220 eV incident energies, and $q > 0$ a.u.

ACKNOWLEDGMENTS

This work was supported by the Australian Research Council and The University of Western Australia. D.K.W. would like to thank Dr. Peter Hayes and Dr. John Flexman for helpful discussions.

-
- [1] I. E. McCarthy and E. Weigold *Electron-Atom Collisions* (Cambridge University Press, Cambridge, 1995).
- [2] M. A. Coplan, J. H. Moore, and J. P. Doering, *Rev. Mod. Phys.* **66**, 985 (1994).
- [3] H. Ehrhardt, K. Jung, G. Knoth, and P. Schlemmer, *Z. Phys. D* **1**, 3 (1986).
- [4] M. Inokuti, *Rev. Mod. Phys.* **43**, 297 (1971).
- [5] I. E. McCarthy, *Z. Phys. D* **23**, 287 (1992).
- [6] I. E. McCarthy and E. Weigold, *Rep. Prog. Phys.* **54**, 789 (1991).
- [7] N. Lermer, B. R. Todd, N. M. Cann, C. E. Brion, Y. Zheng, S. Chakravorty, and E. R. Davidson, *Can. J. Phys.* **74**, 748 (1996).
- [8] A. Pochat, R. J. Tweed, J. Peresse, C. J. Joachain, B. Piraux, and F. W. Byron, *J. Phys. B* **16**, L775 (1983).
- [9] S. Rioual, G. Nguyn Vien, and A. Pochat, *Phys. Rev. A* **54**, 4968 (1996).
- [10] C. T. Whelan, H. R. J. Walters, R. J. Allen, and X. Zhang, in *(e,2e) and Related Processes*, edited by C. T. Whelan, H. R. J. Walters, A. Lahmam-Benanni, and H. Ehrhardt (Kluwer, Dordrecht, 1993), pp. 1–32.
- [11] J. Rösel, K. Jung, H. Ehrhardt, X. Zhang, C. T. Whelan, and H. R. J. Walters, *J. Phys. B* **23**, L649 (1990).
- [12] J. Rösel, C. Dupré, J. Röder, A. Duguet, K. Jung, A. Lahmam-Bennani, and H. Ehrhardt, *J. Phys. B* **24**, 3059 (1991).
- [13] S. Bell, C. T. Gibson, and B. Lohmann, *Phys. Rev. A* **51**, 2623 (1995).
- [14] D. K. Waterhouse, J. F. Williams, and P. A. Smith, *Rev. Sci. Instrum.* **67**, 1769 (1996).
- [15] D. K. Waterhouse and J. F. Williams, *Rev. Sci. Instrum.* **68**, 3363 (1997).
- [16] M. A. Bennett, P. Smith, D. K. Waterhouse, M. J. Ford, J. Flexman, and J. F. Williams, *Rev. Sci. Instrum.* **63**, 1922 (1992).

- [17] A. Lahmam-Bennani, A. Duquet, and C. DalCapello, *J. Electron. Spectrosc. Relat. Phenom.* **40**, 141 (1986).
- [18] M. E. Rudd, K. W. Hollman, J. K. Lewis, D. L. Johnson, R. R. Porter, and E. L. Fagerquist, *Phys. Rev. A* **47**, 1866 (1993).
- [19] I. E. McCarthy, R. Pascual, P. Storer, and E. Weigold, *Phys. Rev. A* **40**, 3041 (1989).
- [20] L. Avaldi, G. Stefani, I. E. McCarthy, and X. Zhang, *J. Phys. B* **22**, 3079 (1989).